

Article

# Electrochemical Instrumentation of an Embedded Potentiostat System (EPS) for a Programmable-System-On-a-Chip

Adrián Iván Muñoz-Martínez <sup>1</sup>, Omar Israel González Peña <sup>1,2,\*</sup>, Jordi Colomer-Farrarons <sup>3</sup>, José Manuel Rodríguez-Delgado <sup>1</sup>, Alfonso Ávila-Ortega <sup>1</sup> and Graciano Dieck-Assad <sup>1</sup>

<sup>1</sup> Tecnológico de Monterrey, Av. Eugenio Garza Sada Sur No. 2501, Col. Tecnológico, Monterrey 64849, Mexico.

<sup>2</sup> Water Center for Latin America and the Caribbean. Av. Eugenio Garza Sada Sur No. 2501, Col. Tecnológico, Monterrey 64849, Mexico.

<sup>3</sup> Department of Electronics, Bioelectronics and Nanobioengineering Research Group (SIC-BIO), University of Barcelona, Martí i Franquès, 08028 Barcelona, Spain.  
adrian.ivan.munoz@gmail.com (A.I.M.M.); jcolomer@el.ub.edu (J.C.F.); jmrdr@itesm.mx (J.M.R.D.); aavila@itesm.mx (A.A.O.); graciano.dieck.assad@itesm.mx (G.D.A.)

\* Correspondence: oig@itesm.mx (O.I.G.P.); Tel.: +52-818-358-2000

**Abstract:** Under the main features required on portable devices in electrochemical instrumentation is to have a small size, low power consumption, economically affordable, and precision in the measurements. This paper describes the development of a programmable Embedded Potentiostat System (EPS) capable of performing electrochemical sensing over system-on-a-chip platforms. Furthermore, the study explains a circuit design and develops some validation of the entire system. The hardware validation is performed by electrochemical experiments such as Double Step Chronoamperometry (DSC), Linear Sweep Voltammetry (LSV) and Cyclic Voltammetry (CV); moreover, a comparison of the experimental signals between a commercial potentiostat and the EPS was done by analysis of errors on the response signal. Results illustrate that the EPS is capable of handling currents in the range of absolute values of 86.44 to 3000 nA, and having control voltages in the range of  $\pm 2$  V. The device can support from 50 to 2000 samples per second. The EPS capabilities were compared with other compact potentiostats. The programmable EPS is an original approach which hugely reduces the hardware complexity and leads the way to create new applications for Point-of-Care or industrial developments with a reusable full electronics module.

**Keywords:** Chronoamperometry, Potential Sweep Methods, Reconfigurable Embedded Potentiostat, Portable Potentiostat, Programmable-System-on-a-Chip, Wireless electronic

## 1. Introduction

Potentiostat is a device which can input predetermined voltage/current signals that generate outputs with an electron-related behavior needed to study redox reactions [1]. The potentiostat also relies on a feedback loop usually implemented with advanced electronic components to accurately control and condition electrical potential differences obtained from sensors to ensure reliable information at the output.

Before the invention of computers to control voltage and/or current, it was challenging to obtain a signal processing in electrochemical instrumentation. Indeed, modern electroanalytical chemistry started with the invention of polarography in the 1920s [2]; since then, the electrochemical instrumentation has been pushing forward according to progress achieved in electronics (Moore's law) and information technology (Internet of Things). Incorporation of electrochemical sensors continues to gain a presence in research efforts to develop technology in different application fields

such as Lab-on-a-chip devices or centrifugal microfluidic platforms [3]; indeed, these microfluidic platforms have proved to be very convenient for clinical diagnosis of glucose and cancer cell detection issues [4-6].

Point of Care Technology (POCT) devices make possible to obtain sample measurements of patients under a large distance. This technology offers features such as shortening the sample analysis periods, reducing the size of the final device reaching portability. Thus, it is possible to implant POCT devices in humans for continuous monitoring purposes [7, 8].

Trends in microelectrode fabrication, microfluidics, and microelectronic systems have resulted in both challenges: in the design/development of potentiostats and significant advances in the capabilities of them to collect data at the transient that take place at different time constants associated to different phenomena.

The lack of the information about the circuitry is one of the most important disadvantages present in commercially supplied potentiostats [9-12]. This information related to electrochemical detection is necessary to manipulate certain variables like the voltage waveforms. Thus, experimentalists have to adapt the methodologies under development to the available potentiostats in the market; likewise, the lack of this information results in different kinds of problems to develop new measurement approaches for the need for highly customized and flexible electrochemical instruments for hardware and software.

This study had proposed a highly customizable and flexible platform consisting of the electronic circuits and the software to drive redox reactions. In addition, it is presented in the study a well-description and characterization on the potentiostat system, which it is necessary for making possible the availability of technological devices [9-13]. Figure 1 shows a possible solution to have a highly customized potentiostat system for applications like Lab-on-a-System, wearable monitoring systems, and POCT. The idea is to have an embedded system small enough to meet the application requirements. In this case, the Programmable System on a Chip (PSoC) and the Programmable Radio on a Chip (PProC) have shown their worth [14-16]. The interface system uses LabVIEW in a computer to deal with the user with a versatile graphical environment [17-21]. The communications between computer and PSoC is wireless. The scalability of the system takes place using pattern designs at the software level.

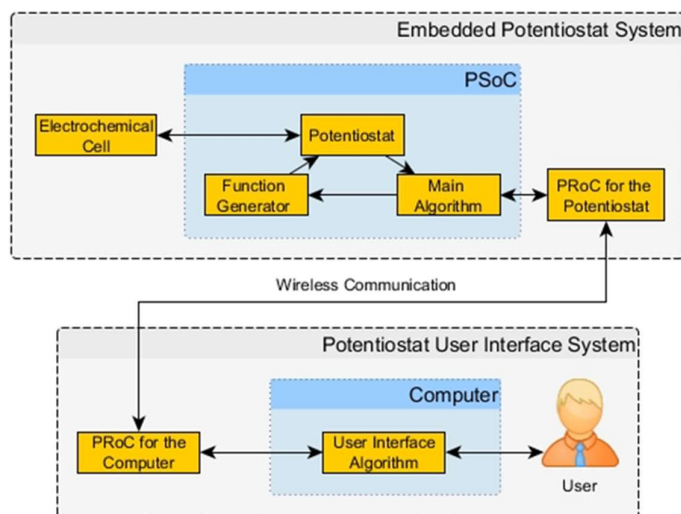


Figure 1. Block Diagram of the Embedded Potentiostat System (EPS) with its User Interface.

Furthermore, it is presented in this work a flexible and integral methodology that includes the characterization and calibration of the potentiostat, thus the electronics of the device were tested by performing three electrochemical techniques and its analysis of errors. This methodology allows for the reconfiguration of the device to execute different electrochemical techniques allowing a correct functioning of the equipment.

## 1.2. Background

A potentiostat by itself just controls the potential in an electrochemical cell, and more electronic components are necessary to get more information about the electrochemical phenomenon [22-23]. The Digital to Analog Converter (DAC) provides the control signal for the potentiostat. The current measurement circuit reads the electrons flow of the reactions. The Analog to Digital Converter (ADC) turns the analog current values in digital. Thus, the basic potentiostat system defines the performance of the entire instrument. The prototype implementation and architecture of the digital peripherals and analog circuitry of the PSoC is possible to observe in detail into the supplementary materials of this study.

The function generator can give the waveform values in an analog or digital way. However, a computer generates the digital signals most of the time. Also, the recorder system has to handle digital values because it is the easiest way to save data. The display system can be any device capable of showing information. Though, one of the fastest is a screen. Hence, all these components and the basic potentiostat system let us have a complete device to perform electrochemical experiments.

## 2. Materials and Methods

### 2.1. Electrochemical equipment

The EPS uses two kits as it is shown on figure 5 from Cypress Semiconductors: CY8CKIT-059 and CY8CKIT-042-BLE, the CY8CKIT-059 kit has the chip CY8C5888LTI-LP097; the CY8CKIT-042-BLE kit has four devices, but the prototype just needs the PSoC and the USB dongle. The measurements of the EPS are compared to a commercial potentiostat system (CH Instruments, model 700E). The EPS was operated to recording 2000 data per second which is the maximum samples that the equipment can measure. The three cables on figure 2 at the bottom right part of the protoboard were connected to the three electrodes of the electrochemical cell.

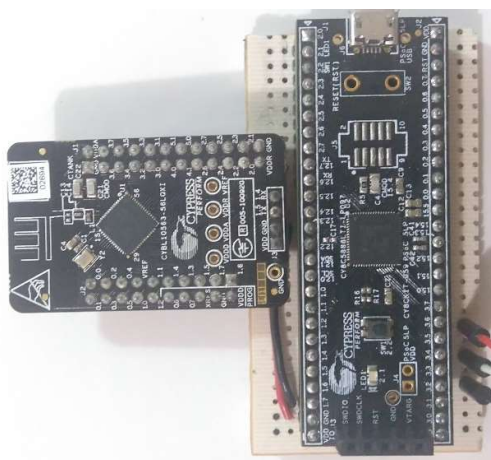
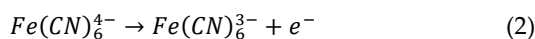


Figure 2. Prototype of the EPS.

### 1.2. Analyte, Electrolyte and Electrodes

All experiments were performed on a volume of 50 mL of potassium ferricyanide  $K_3[Fe(CN)_6]$ ; this analyte is common to use to test potentiostats [11, 24 - 26], since its kinetics is well known, and it describes an electrochemical reversible behavior [22, 27, 28]. Ferricyanide can be reduced to

ferrocyanide as equation 1 shows; the backward direction of the reaction corresponds to the ferrocyanide oxidation to ferricyanide as equation 2 describes.



In the experiments two analyte concentrations of 1 mM and 10 mM of  $K_3[Fe(CN)_6]$  (Sigma-Aldrich, CAS: 13746-66-2) were used to evaluate the EPS. The electrolyte support used was 0.5 M KCl (Fermont, presentation no. 24842). The reference electrode (RE) used is Ag/AgCl (BASi model MF-2052). Platinum wire (BASi model MW-4130), and a disk glassy carbon electrode (BASi model MF-2012, diameter  $\phi = 3$  mm) was used as the Counter electrode (CE), and Working Electrode (WE), respectively.

### 1.3. Experimental Design

The electrochemical techniques used in the EPS are LSV, CV, and DSC. Before to do a comparison of the commercial potentiostat with the EPS, the WE were cleaned by immerse it in 0.1 M of  $HNO_3$  (sigma aldrich) for approximately 10 minutes, later the WE was rinsing with distilled water; after that, the WE received an electrochemical pretreatment to activate its surface by running a sequence of different scan rates of CV and by using 0.1M of HCl (sigma aldrich); The CV sequences of the activation surface is shown on table I.

Table I: Sequences for the surface activation on the WE.

	sequence 1	sequence 2	sequence 3	sequence 4
<b>Scan Rate</b>	500 mV/s	250 mV/s	100 mV/s	50 mV/s
<b>Cycles</b>	50	25	10	5
<b>Method</b>	Cyclic Voltammetry			
<b>Initial Voltage</b>	0.25 V			
<b>Maximum Voltage</b>	0.65 V			
<b>Minimum Voltage</b>	-0.15 V			
<b>Initial Scan Direction</b>	anodic direction			

The process of surface activation is initiating with a high scan rate (500 mV/s) and through lower scan rates until reach a scan rate of (50 mV/s). In the process of the surface activation, all CVs were done on the windows of scan potentials of (-0.15 to 0.65) V vs Ag/AgCl where the initial voltage was set at 0.25V vs Ag/AgCl. Likewise, the number per cycles of each sequence of CV is higher (50 cycles) at the highest scan rate and it decreases at lower scan rates until reach (5 cycles). All experiments were carried out at room temperature  $\sim 25^\circ C$  and the potential recorded were against the Ag/AgCl saturated.

The Randles-Sevcik equation presented below relates the scan rate, the molecular diffusion and bulk concentration of the analyte with the current peak from a CV or LSV experiments [28, 29].

$$I_p = (2.69 \times 10^5) n^{3/2} (Dv)^{1/2} AC^{bulk} \quad (3)$$

Here,  $I_p$  is the maximum current (A),  $n$  is the number of electrons per mole oxidized or reduced,  $D$  is the diffusion coefficient ( $\text{cm}^2/\text{s}$ ),  $v$  is the scan rate of the CV or LSV ( $\text{V}/\text{s}$ ),  $A$  is the working electrode area ( $\text{cm}^2$ ), and  $C^{bulk}$  is the bulk concentration of the oxidized or reduced specie ( $\text{mol cm}^{-3}$ ). Table II shows the parameters of the Randles-Sevcik equation and the current peaks of the two concentrations tested in an ideal Nernstian reversible system and under the assumption of semi-infinite linear diffusion.

Table II: Randles-Sevcik parameters and expected maximum current from CV and LSV experiments.

	Solution 1	Solution 2
<b><math>\text{K}_3[\text{Fe}(\text{CN})_6]</math>, analyte concentration</b>	1 mM	10 mM
<b>KCl, Electrolyte support concentration</b>		0.5 M
<b># of e<sup>-</sup> per mole oxidized or reduced</b>		1
<b>Analyte Diffusion Coefficient</b>		7.23 $\mu\text{cm}^2/\text{s}$ [30]
<b>Scan Rate</b>		10 mV/s
<b>Room Temperature</b>		25 °C
<b>Surface Area of WE</b>		0.071 $\text{cm}^2$
<b>Randles-Sevcik Current Peak</b>	5.11 $\mu\text{A}$	51.1 $\mu\text{A}$

The setup condition for each experiment has been related to the number of the experimental conditions. The conditions rely on the previous investigation where similar values were used [9, 13]. The only changes between conditions were the scan rate value. Hence, conditions allow us to evaluate the EPS at different currents magnitudes and scan rates. In addition, a comparison was done of the EPS signal with a commercial potentiostat. Table III describes the setup parameters for the conditions tested on CVs.

Table III: CV conditions for each experiment.

	Condition 1	Condition 2	Condition 3	Condition 4
<b>Scan Rate</b>	10 mV/s	100 mV/s	250 mV/s	500 mV/s
<b>Initial Voltage</b>			0.25 V	
<b>Minimum Voltage</b>			-0.15 V	
<b>Maximum Voltage</b>			0.65 V	
<b>Recorded cycle for comparison</b>			fifth	
<b>Initial Scan Direction</b>			anodic direction	
<b>Analyte concentration</b>			1 mM $\text{K}_3[\text{Fe}(\text{CN})_6]$	
<b>Electrolyte support concentration</b>			0.5 M KCl	

Table IV describes the conditions for the DSC experiments. The small changes between the first and the last step allow us to explore the changes in the current measurements on the prototype and it can be related to the lowest limit of detection on the device. The pulse width was set to 62 seconds since at that time the current measurement reaches the steady-state response. The last step is practically the open circuit potential of 0.308 V for 1 mM  $\text{K}_3[\text{Fe}(\text{CN})_6]$  in Table 3.

Table IV: DSC conditions for each experiment.

	Cond. 5	Cond. 6	Cond. 7	Cond. 8	Cond. 9
<b>First Step</b>	0.325 V	0.315 V	0.305 V	0.295 V	0.195 V
<b>Last Step</b>			0.310 V		
<b>Pulse Width</b>			62 seconds		
<b>Quite time</b>			62 seconds		
<b>Analyte</b>			1 mM $K_3[Fe(CN)_6]$		
<b>Electrolyte</b>			0.5 M KCl		

Table V describes the conditions for the LSV experiments. The conditions rely on the previous investigation where similar values were used [9, 13], where the only changes were the scan rates.

Table V: LSV conditions for the experiments.

	Cond. 10	Cond. 11	Cond. 12	Cond. 13	Cond. 14	Cond. 15
<b>Initial Voltage</b>	0.65 V	-0.15 V	0.65 V	-0.15 V	0.65 V	-0.15 V
<b>Final Voltage</b>	-0.15 V	0.65 V	-0.15 V	0.65 V	-0.15 V	0.65 V
<b>Scan Rate</b>	10 mV/s	10 mV/s	100 mV/s	100 mV/s	500 mV/s	500 mV/s
<b>Analyte</b>			1 mM $K_3[Fe(CN)_6]$			
<b>Electrolyte</b>			0.5 M KCl			

### 3. Results and Discussion

Results of the experimental conditions in tables III, IV and V are in the graphs from Figure 3 to Figure 5. In the LSV and CV, the voltage values are versus the RE, and it is indicated as EREF on the abscissa axis. All electrochemical experiments follow the sign convention used on the commercial potentiostat (chemistry convention); therefore, the peak currents observed on CVs in figure 3 with negative magnitude, correspond to the oxidation in the equation 2; contrary, the positive magnitude of the current corresponds to a reduction in the equation 1. A minor discrepancy on the signal of the prototype occurred at high currents; however, the results from the prototype are close to the commercial potentiostat in most of the graphs when it is considered a proper range to work for the prototype. A minor drawback of the potentiostat prototype is the filter; this capacitor introduces a shift phase, and it is possible to be observed when the scan rate is fast as Figure 3(D) shows. This filter is necessary because noise appears in the measurements specially when very low currents are monitored. Thus, this component allows us to reduce the detection limits sacrificing a little of the potentiostat prototype bandwidth.

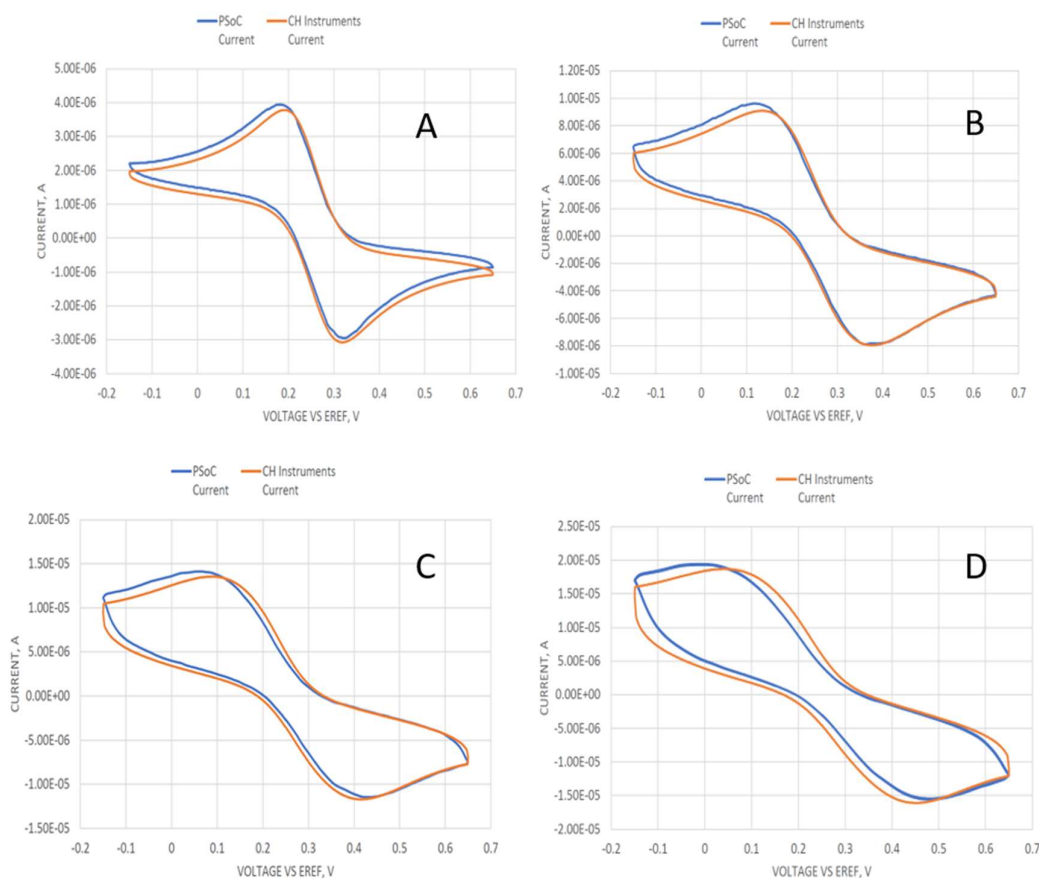


Figure 3: Cyclic voltammetry at different scan rates of 1 mM  $K_3[Fe(CN)_6]$  and 0.5 M KCl as the electrolyte support; the working electrode, the counter electrode and the reference electrode were a disk glassy carbon electrode (diameter  $\phi = 3$  mm), a platinum wire and Ag/AgCl electrode, respectively: (A) 10 mV/s (experiment under the conditions 1). (B) 100mV/s (experiment under the conditions 2). (C) 250 mV/s (experiment under the conditions 3). (D) 500 mV/s (experiment under the conditions 4).

In figure 4, it is shown different DSCs at different first step potentials described in Table IV. In figure 4 (A and B), the initial step corresponds to the oxidation, and on the second step it is shown a reduction; contrary, in figures 4(C, D, and E) the process has been inverted.

In figures 4(B and C), the current recorded at longer times describes more evidently an oscillation when the system is close to reach a relaxed response; This oscillation can be related to the perturbation step signal, which was very close to the open circuit potential; as a result, in figures 4(B and C), the ratio of the peak currents divided by the current measured at the steady-state provides a less abrupt ratio compared when the system is under a large perturbation signal of a given step of potential.

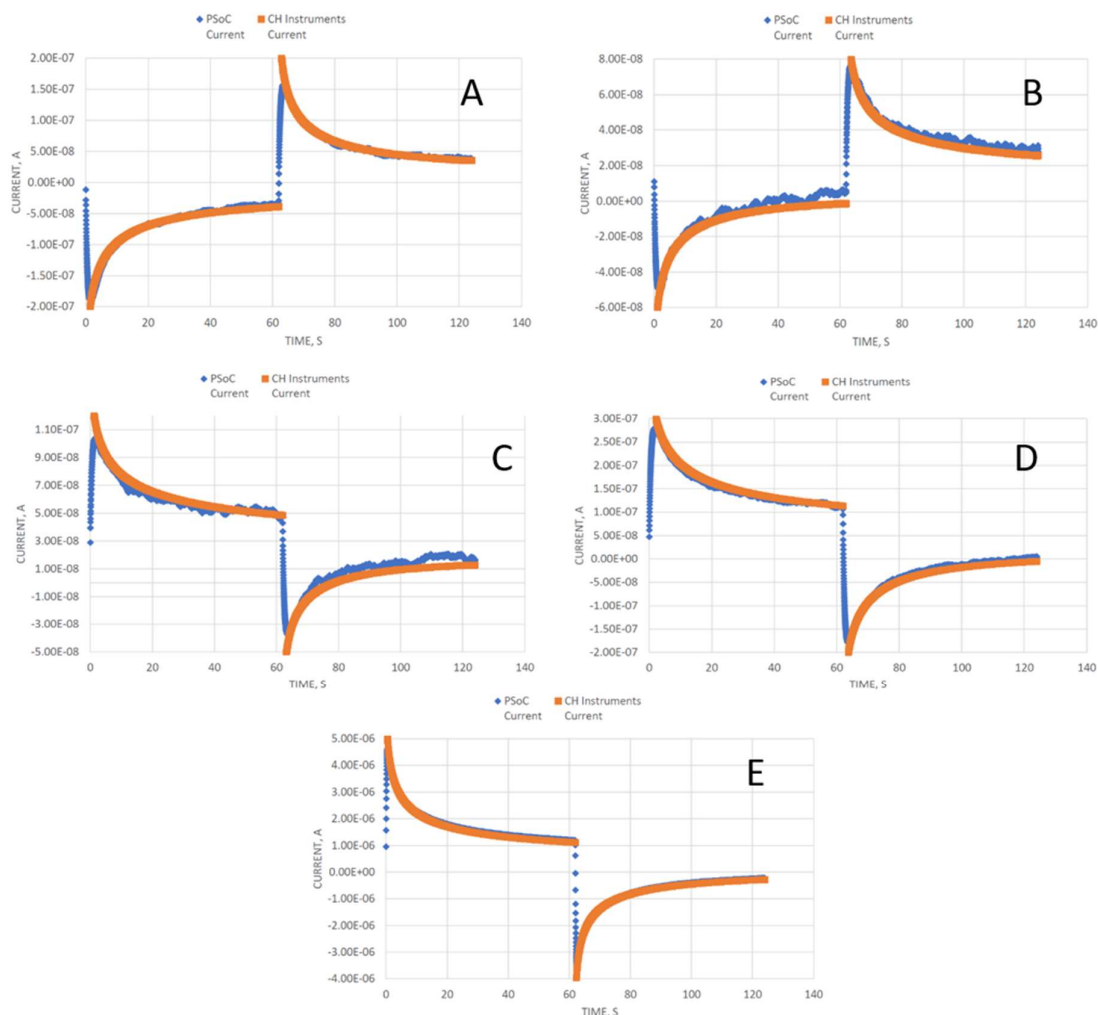


Figure 4: Double Step Chronoamperometry at different first step potentials of 1 mM  $K_3[Fe(CN)_6]$  and 0.5 M KCl as the electrolyte support; the working electrode, the counter electrode and the reference electrode were a disk glassy carbon electrode (diameter  $\phi = 3$  mm), a platinum wire, and Ag/AgCl electrode, respectively. All DSC were done with a pulse width of 62 seconds and the last step was setup at 0.310 V vs Ag/AgCl: (A) first step potential 0.325 V vs Ag/AgCl (experiment under the conditions 5). (B) first step potential 0.315 V vs Ag/AgCl (experiment under the conditions 6). (C) first step potential 0.305 V vs Ag/AgCl (experiment under the conditions 7). (D) first step potential 0.295 V vs Ag/AgCl (experiment under the conditions 8). (E) first step potential 0.195 V vs Ag/AgCl (experiment under the conditions 9).

In figure 5, it is shown LSV experiments described in table V. In figures 5(A, C, and E), it is shown LSV under a cathodic scan and corresponds to a reduction; on the other hand, in figures 5(B, D, and F), it is shown the anodic direction on the LSV associated with an oxidation. A little discrepancy of the phase response was observed at the maximum scan rate of 500 mV/s for the cathodic and anodic directions with respect to the commercial potentiostat response; The little difference can be associated with the same signal observed at the highest scan rate of the CV experiment.

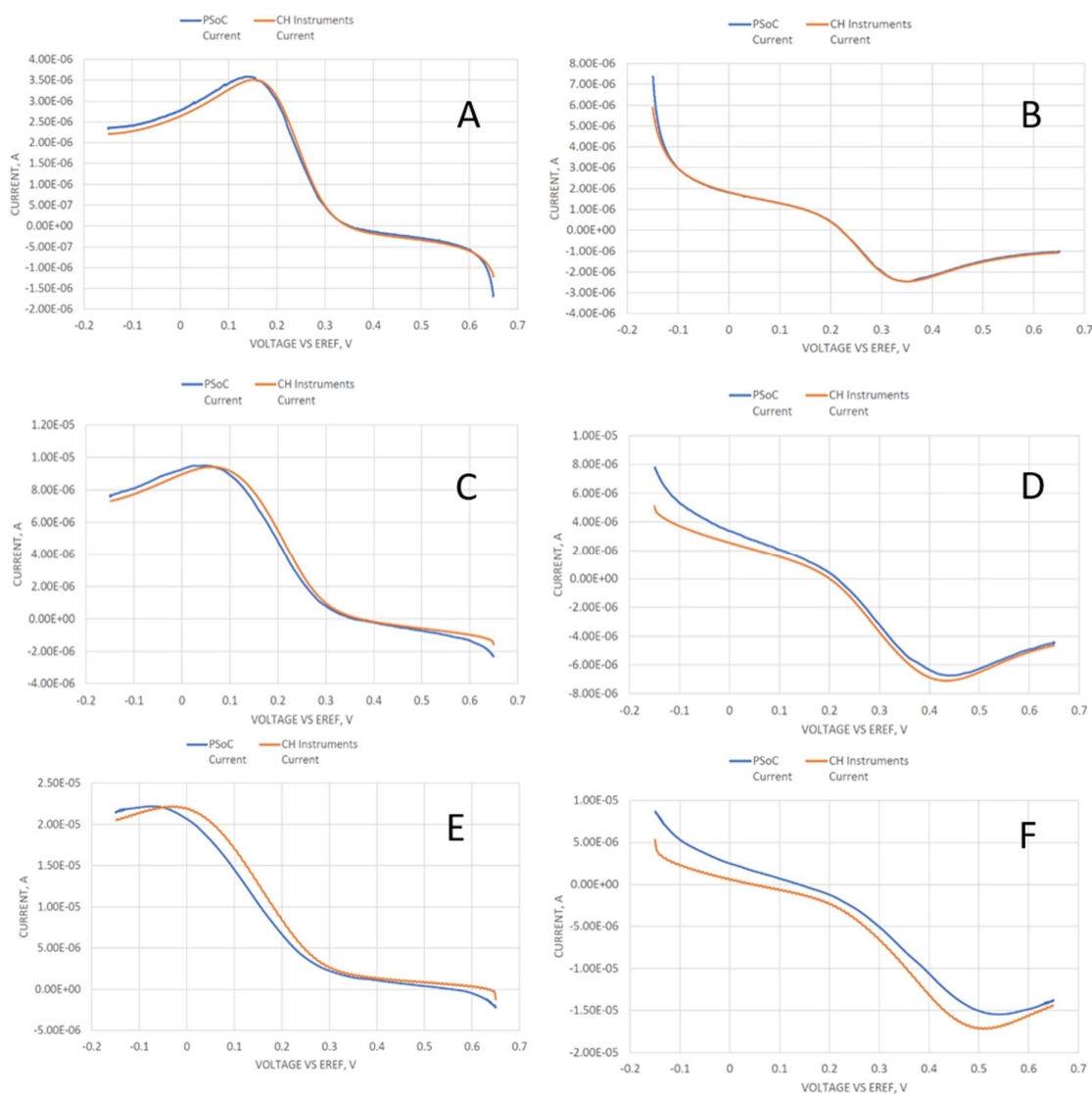


Figure 5: Linear sweep voltammetry at different scan rates at different first step potentials of 1 mM  $K_3[Fe(CN)_6]$  and 0.5 M KCl as the electrolyte support; the working electrode, the counter electrode, and the reference electrode were a disk glassy carbon electrode (diameter  $\phi = 3$  mm), a platinum wire and Ag/AgCl electrode, respectively. All voltages are reported vs Ag/AgCl. (A) Scan rate 10 mV/s, initial and final voltage are 0.65V and -0.15V, respectively (experiment under the conditions 10). (B) Scan rate 10 mV/s, initial and final voltage are -0.15V and 0.65V, respectively (experiment under the conditions 11). (C) Scan rate 100 mV/s, initial and final voltage are 0.65V and -0.15V, respectively 12). (D) Scan rate 100 mV/s, initial and final voltage are -0.15V and 0.65V, respectively (experiment under the conditions 13). (E) Scan rate 500 mV/s, initial and final voltage are 0.65V and -0.15V, respectively (experiment under the conditions 14). (F) Scan rate 500 mV/s, initial and final voltage are -0.15V and 0.65V, respectively (experiment under the conditions 15).

### 3.1. Analysis of Results

An error analysis will show the differences between both devices for each experiment quantitatively. The absolute error express how far is the measured value of the real as the equation 4 describes. In these experiments, the real values are from the commercial potentiostat while the measured values are from the prototype. The mean error refers to the average of the absolute errors in an experiment

as equation 5 agrees. The highest error is a value very close to the maximum error because it comes from the standard deviation ( $\sigma$ ) of the absolute errors as equation 6 shows.

$$\text{Absolute Error} = \left| |Value_{Measured}| - |Value_{Real}| \right| \quad (4)$$

$$\text{Mean Error} = \frac{\sum_{i=1}^{\text{Sample Number}} (\text{Absolute Error})_i}{\text{Sample Number}} \quad (5)$$

$$\text{Highest Error} = 3\sigma + \text{Mean Error} \quad (6)$$

The previous equations do not have any reference to describe the error and with this peculiarity, it cannot be clear how bad is that error. Thus, the full scale will be the reference with a value according to the peak to peak amplitude of the Redox current signal from the commercial potentiostat. The Mean Error Percent (MEP) describes how big the mean error is against the peak to peak amplitude as equation 7 illustrates. The Highest Error Percent (HEP) describes how big this highest error is against the peak to peak amplitude as equation 8 shows. Hence, these indicators will describe the error of the prototype measurements with a solid reference.

$$\text{Mean Error Percent} = \frac{\text{Mean Error}}{\text{Peak to Peak Amplitude}} * 100 \quad (7)$$

$$\text{Highest Error Percent} = \frac{\text{Highest Error}}{\text{Peak to Peak Amplitude}} * 100 \quad (8)$$

It is shown in Table VI the most relevant indicators for the error analysis. The MEP describes the error percent to expect in given measure. The HEP describes maximum error percent to expect in an electrochemical trial. The CV errors are higher than those from the DSC, and that can come from two factors: the full scale and the scan rate. However, it is difficult to know which of both has more weight because they are related.

Table VI: Error analysis summary of the CV, DSC and LSV experiments in figures 3-5, and by using equations 4- 8. Experimental conditions are reported in tables III-V.

Experiment under the:	MEP, %	HEP, %	Mean Error, A	Highest Error, A	Full Scale, A	Method
Conditions 1	2.887	5.226	1.98E-07	3.58E-07	6.852E-06	CV
Conditions 2	1.691	5.721	2.88E-07	9.75E-07	1.704E-05	CV
Conditions 3	2.226	7.653	5.62E-07	1.93E-06	2.527E-05	CV
Conditions 4	<b>3.397</b>	<b>11.178</b>	1.18E-06	3.89E-06	3.481E-05	CV
Conditions 5	0.319	5.185	5.35E-09	8.69E-08	1.676E-06	DSC
Conditions 6	0.587	5.386	<b>3.6E-09</b>	3.30E-08	<b>6.134E-07</b>	DSC
Conditions 7	<b>0.780</b>	5.480	<b>5.04E-09</b>	3.54E-08	<b>6.461E-07</b>	DSC
Conditions 8	0.562	<b>6.169</b>	1.03E-08	1.13E-07	1.827E-06	DSC
Conditions 9	0.414	4.758	7.73E-08	8.87E-07	1.865E-05	DSC

<b>Conditions 10</b>	2.019	5.994	9.55E-08	2.83E-07	4.728E-06	LSV
<b>Conditions 11</b>	0.585	5.464	4.88E-08	4.56E-07	8.341E-06	LSV
<b>Conditions 12</b>	2.837	8.429	3.12E-07	9.26E-07	1.098E-05	LSV
<b>Conditions 13</b>	5.081	17.825	6.2E-07	2.18E-06	1.220E-05	LSV
<b>Conditions 14</b>	4.243	14.483	9.94E-07	3.39E-06	2.342E-05	LSV
<b>Conditions 15</b>	<b>7.655</b>	<b>19.173</b>	1.72E-06	4.32E-06	2.252E-05	LSV

The experimental conditions 6 and 7 allow knowing the resolution of the equipment that can be related to the Lower Limit of Detection (LLD), thus in these trials the prototype measured the smallest signal value. From the conditions 6 and 7, it is possible to calculate the 5% of the mean error. Therefore, its values reflex the LLD to have an expected accuracy of 95% in the measurements compared with the commercial potentiostat. With that criterion, *“the prototype can handle currents above 86.44 nA and below of -86.44 nA”*, as Table VII shows to have an accuracy above of the 95%.

Table VII: Lower Limit of Detection analysis.

	<b>Mean Error, A</b>	<b>LLD from 5% of the Mean Error, A</b>
<b>Conditions 6</b>	3.6E-09	***
<b>Conditions 7</b>	5.04E-09	***
<b>Conditions Average</b>	4.32E-09	86.44E-09

To obtain the Higher Limit of Detection (HLD) an additional experiment was carried out at the experimental conditions described in Table VIII (condition 16) and it is presented in figure 6.

Table VIII: Condition to explore the highest limit of detection.

<b>Conditions 16</b>	
<b>Scan Rate</b>	10 mV/s
<b>Initial Voltage</b>	0.40 V
<b>Minimum Voltage</b>	-0.10 V
<b>Maximum Voltage</b>	0.53 V
<b>Cycle</b>	Fifth
<b>Initial Scan Direction</b>	Positive
<b>Analyte</b>	10 mM $K_3[Fe(CN)_6]$
<b>Electrolyte Support</b>	0.5 M KCl

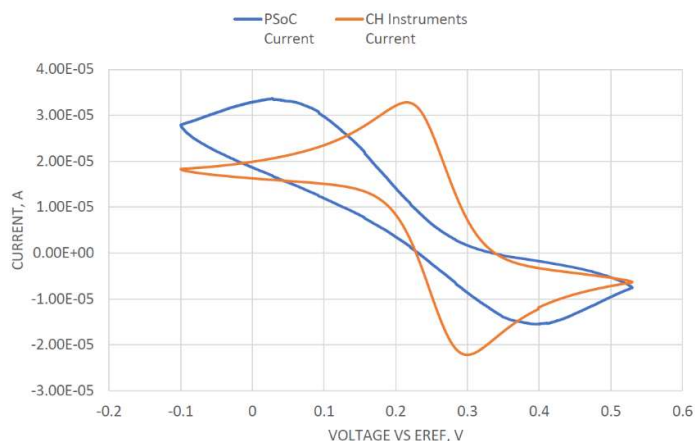


Figure 6: Cyclic voltammetry at 10mV/s, 10 mM  $K_3[Fe(CN)_6]$  and 0.5 M KCl as the electrolyte support; the working electrode, the counter electrode and the reference electrode were a disk glassy carbon electrode (diameter  $\phi = 3$  mm), a platinum wire, and Ag/AgCl electrode, respectively; experiment under the conditions 16: (Blue line) CV response by the EPS. (Orange line) CV response by the commercial potentiostat.

The HLD comes from the current values of the CV; in specific, the condition 16 shows how the prototype cannot handle much current. The main difference between experimental conditions 1 and 16 is the concentration difference in the analyte (10 times in the order of magnitude). The figure 9 describes how the EPS response is under a different phase than the commercial potentiostat. The condition one provides the HLD of  $\pm 3 \mu A$  according to the possible resolution of the system. However, trials with analyte concentration between (1 and 10) mM  $K_3[Fe(CN)_6]$  could prove a greater current range.

## 5. Conclusions

Table IX shows the electrochemical conditions where the response signal of the prototype is congruent with the commercial potentiostat. This table is a summary of the experiments to appreciate the capacity of the EPS. The concentration used provides information about the voltage and the current range of the electrochemical techniques studied. In addition, the study provides a guide to test the scan rate and the range of the sample per second on the EPS.

Out of the ranges of Table IX, the behavior of the EPS is erratic or unknown. The potentiostat loses the voltage control with analyte concentrations above 10 mM  $K_3[Fe(CN)_6]$ . As a result, the EPS capacity established in this study allows us to have several applications for the medical, biotechnology, environmental areas.

Table IX: Electrochemical conditions evaluated.

	CV	LSV	DSC
Analyte Concentration	1 mM $K_3[Fe(CN)_6]$	1 mM $K_3[Fe(CN)_6]$	1 mM $K_3[Fe(CN)_6]$
Voltage Range	-0.15 to 0.65 V	-0.15 to 0.65 V	0.195 to 0.325 V
Peak Current Range	-3.0 to 4.0 $\mu A$	-2.5 to 3.5 $\mu A$	***
Maximum Step	***	***	0.310 to 0.195 V
Minimum Step	***	***	0.310 to 0.315 V
Maximum Current at 62 seconds	***	***	1.2 $\mu A$
Minimum Current at 62 seconds	***	***	43.22 nA
Scan Rate Range	10 to 500 mV/s	10 to 500 mV/s	***
SPS Range	50 to 2000 SPS	50 to 2000 SPS	50 to 2000 SPS

Table X describes the principal features of the EPS. The prototype has a capacity of  $\pm 2$  V to control the voltage. The range of currents was established from the experiments discussed previously. The number of samples per seconds comes from the ADC selected in the PSoC. The scan rate range relies on the architecture of the PSoC and the algorithm that controls the waveform generator. The parameters described in table 10 point out that the PSoC is a suitable device to work as a prototype of a portable EPS.

Table X: Principal electric features of the EPS.

Voltage Range: $\pm 2$ V	Samples per Second: <b>50 to 2000</b>
Current Range: $\pm 3$ $\mu A$	Scan Rate: <b>10 to 500 mV/s</b>

Tables XI and XII give information about the power consumption and the values to compensate for having more accurate results. The offset voltages are summarized in Table IX and the bias current at the inverting input establishes the minimum current to read in the device. The power consumption provides a clear idea of the battery requirements.

Table XI: Additional features of the EPS with a source voltage of 5 volts.

ADC Offset Voltage: <b>-61.056 <math>\mu V</math></b>	EPS consumption at Stand By: <b>137.5 mW</b>
TIA Offset Voltage: <b>-3.36034 mV</b>	EPS consumption at 2000 SPS: <b>207.5 mW</b>

Table XII. TIA resistor calculated and bias current at the inverting input.

TIA Resistors	Value Calculated	Bias Current at the inverting input
R1	18971.46 $\Omega$	3.40E-08 A
R2	28636.77 $\Omega$	2.06E-08 A
R3	38272.14 $\Omega$	1.67E-08 A

R4	77433.47 $\Omega$	6.77E-09 A
R5	116828.09 $\Omega$	5.35E-09 A
R6	244583.12 $\Omega$	2.59E-09 A
R7	490370.41 $\Omega$	1.27E-09 A
R8	981623.90 $\Omega$	6.89E-10 A

#### 4.1. Potential applications of the EPS developed

According to Periasamy et. al., it is possible to use their glucose biosensor in a linear concentration range of 6.3 to 20.09 mM [40], and the concentration can go from 2 to 22 mM in humans [31]. The biosensor has a sensitivity of 2.47  $\mu\text{A}/(\text{mM cm}^2)$ . In addition, the output current range of the biosensor with a fixed area of 2 mm  $\times$  2 mm is of 0.62 to 1.98  $\mu\text{A}$ . Hence, this prototype can handle that sensor because the EPS input current is wider than the biosensor output.

Apetrei. et. al. developed a sensor with a sensitivity of 37.1 nA/ $\mu\text{M}$  with an area of 0.867  $\text{cm}^2$  in a linear range of 1-300  $\mu\text{M}$  to detect melatonin [32]. With the EPS it is possible to detect melatonin in a concentration of 43  $\mu\text{M}$ , since the detection range is around 2.5-80.0  $\mu\text{M}$ .

Other works have developed sensors with a sensitivity of 35 mA/(M  $\text{cm}^2$ ) for  $\text{H}_2\text{O}_2$  [33-35]. In an amount of 10-200  $\mu\text{M}$ , it can provoke a senescence-like state if a human cell gets in contact with it [35]. Thus, in a fixed area of 7.2mm  $\times$  7.2mm it is possible to detect it in a range of 5-165  $\mu\text{M}$  with the EPS.

Jaiswal et. al. developed a biosensor for the determination of nitrite ( $\text{NO}_2^-$ )[36]. In that study, they found two linear ranges of 0.1 to 1  $\mu\text{M}$  and 1 to 1000  $\mu\text{M}$  having two different sensitivities of 1.25  $\mu\text{A}/(\mu\text{M cm}^2)$  and 0.005  $\mu\text{A}/(\mu\text{M cm}^2)$ , respectively. As a result, the EPS can be useful in the detection of nitrite in a range of 0.1 to 833  $\mu\text{M}$  with an electrode area of 0.72  $\text{cm}^2$  and by considering the two slopes in this range.

Furthermore, the EPS can accomplish suitable features such as being a compact device, have a low power consumption, economically affordable ( $\sim$ \\$100 USD), flexible for being programmed according to with the required necessity, suitable for being integrated over system-on-a-chip platforms, it provides accuracy in the range of measured currents. In addition, since there is a setup of slave-master on the EPS, then it becomes attractive to use this technology to install a network of different EPS to transmit via wireless communication the sensing data to the Potentiostat User Interface System (PUIS).

Finally, in table XIII and XIV it is shown a comparison of different compact potentiostats that has been studied to visualize their parameters to the parameters that can offer the EPS studied.

Table XIII: Electrochemical Instruments Comparison.

Electrochemical Instrument	Jafari et. al. [37]	Dorta-Quinones et. al. [38]	Bozorgzadeh et. al. [39]	Dryden et. al. [9]
Highest Current	350 nA	430 nA	950 nA	22 mA
Detection Limit				

<b>Lowest Current Detection Limit</b>	8.6 pA	***	***	600 fA
<b>Electronic Chip Area</b>	3 mm x 3 mm	1.5 mm x 1.0 mm	3.16 mm x 3.16 mm	***
<b>PCB Area</b>	***	4.7 cm x 1.9 cm	***	8 cm x 8 cm
<b>Maximum Samples Per Second</b>	2 ksps	10 ksps	10 ksps	30 ksps
<b>ADC Effective Number of Bits</b>	9 bits	10.95 bits	***	21.3 bits at 1.45 ksps
<b>Wireless Connectivity</b>	Ultra-Wideband Transmitter	Ultra-Wideband Transmitter	FSK Transmission with Manchester Encoding	No
<b>Number of Techniques Implemented</b>	1	1	2	More than 3
<b>Channels</b>	54	1	1	1
<b>SoC Present</b>	Yes	Yes	Yes	No
<b>Capabilities additional to a potentiostat</b>	No	No	No	Yes
<b>Maximum Power Consumption</b>	1543.3 $\mu$ W for each channel	30 $\mu$ W	Approximately 0.4 mW	Less than 1 W

Table XIV: Electrochemical Instruments Comparison (Continuation).

<b>Electrochemical Instrument</b>	<b>EmStat 3+ Embedded / OEM [40]</b>	<b>WaveNow AFTP1 [41]</b>	<b>Sun et. al. [10]</b>	<b>Giordano et. al. [42]</b>
<b>Highest Current Detection Limit</b>	100 mA	100 mA	200 $\mu$ A	50 $\mu$ A
<b>Lowest Current Detection Limit</b>	1 pA	80 nA	1 nA	100 nA
<b>Electronic Chip Area</b>	***	***	***	***
<b>PCB Area</b>	5.5 cm x 4.1 cm	16.5 cm x 10 cm	3.9 cm x 1.62 cm	9.7 x 5.7 cm

<b>Maximum Samples Per Second</b>	Less than 1 Ksps	1 Ksps	200 ksps	***
<b>ADC Effective Number of Bits</b>	***	***	***	***
<b>Wireless Connectivity</b>	Bluetooth or Wifi	No	No	Bluetooth
<b>Number of Techniques Implemented</b>	9	33	3	4
<b>Channels</b>	up to 16	1	2	1
<b>SoC Present</b>	***	***	No	No
<b>Capabilities additional to a potentiostat</b>	Yes	Yes	Yes	No
<b>Maximum Power Consumption</b>	2.5 W	10 W	111 mW	***

**Supplementary Materials:** The following are available online at [www.mdpi.com/xxx/s1](http://www.mdpi.com/xxx/s1), Figure S1: title, Table S1: title, Video S1: title.

**Author Contributions:** wrote the code for the EPS, and performed experiments to evaluate the electronics on the EPS and for the electrochemical experiments, A.I.M.M.; performed experiments for the electrochemical experiments, analyzed the results, proposed the experimental methodology and setup conditions, wrote the article, O.I.G.P.; proposed the methodology for evaluating the errors and precision on the EPS, J.C.F.; developed the architecture circuit design on the potentiostat, J.M.R.D.; reviewed the code written for the EPS, A.A.O.; reviewed the overall functionality of the EPS from the point of view of the embedded electronics, funding acquisition, G.D.A.

**Funding:** This research was funded by Tecnológico de Monterrey and was funded by The National Council of Science and Technology of Mexico (CONACYT).

**Acknowledgments:** The National Council of Science and Technology of Mexico (CONACYT) and the Tecnológico de Monterrey provided financial support to conduct this study.

**Conflicts of Interest:** The authors declare no conflict of interest. The founding sponsors had no role in the design of the study; in the collection, analyses, or interpretation of data; in the writing of the manuscript; or in the decision to publish the results.

## References

- [1] Allen. J. Bard and Larry. R. Faulkner, "Electrochemical Instrumentation," in *Electrochemical Methods: Fundamentals and Applications*, John Wiley & Sons (New York), 2001, pp. 632–658.
- [2] Evgeny Katz, "Processing electrochemical signals at both sides of interface: electronic vs. chemical signal processing", *J Solid State Electrochem* (2011) 15:1471–1480.
- [3] Madou, M., Zoval, J., Jia, G., Kido, H., Kim, J., & Kim, N. (2006). "LAB ON A CD". *Annual Review of Biomedical Engineering*, 8(1), 601–628.
- [4] J. Höfflin, S. M. Torres Delgado, F. Suárez Sandoval, J. G. Korvink, and D. Mager, "Electrifying the disk: a modular rotating platform for wireless power and data transmission for Lab on a disk application.," *Lab Chip*, vol. 15, no. 12, pp. 2584–7, 2015.
- [5] K. Abi-Samra, T.-H. Kim, D.-K. Park, N. Kim, J. Kim, H. Kim, Y.-K. Cho, and M. Madou,

- “Electrochemical velocimetry on centrifugal microfluidic platforms,” *Lab Chip*, vol. 13, no. 16, pp. 3253–60, Aug. 2013.
- [6] C. E. Nwankire, A. Venkatanarayanan, T. Glennon, T. E. Keyes, R. J. Forster, and J. Ducreé, “Label-free impedance detection of cancer cells from whole blood on an integrated centrifugal microfluidic platform,” *Biosens. Bioelectron.*, vol. 68, pp. 382–389, 2015.
- [7] E. Juanola-Feliu, P. L. Miribel-Catala, C. P. Aviles, J. Colomer-Farrarons, M. Gonzalez-Pinero, and J. Samitier, “Design of an implantable nano-enabled biomedical device for in-vivo glucose monitoring,” in *Design of Circuits and Integrated Systems*, 2014, pp. 1–6.
- [8] J. Colomer-Farrarons, P. Miribel-Català, I. Rodríguez-Villarreal, and J. Samitier, “Portable Bio-Devices: Design of electrochemical instruments from miniaturized to implantable devices,” *New Perspect. Biosens. Technol. Appl.*, pp. 1–458, Jul. 2011.
- [9] M. D. M. Dryden and A. R. Wheeler, “DStat: A versatile, open-source potentiostat for electroanalysis and integration,” *PLoS One*, vol. 10, no. 10, p. 17, Oct. 2015.
- [10] A. Sun, A. G. Venkatesh, and D. A. Hall, “A Multi-Technique Reconfigurable Electrochemical Biosensor: Enabling Personal Health Monitoring in Mobile Devices,” *IEEE Trans. Biomed. Circuits Syst.*, 10(5) 945–954, 2016.
- [11] T. Luo, H. Wang, H. Song, and J. B. Christen, “CMOS potentiostat for chemical sensing applications,” in *IEEE SENSORS 2013 - Proceedings*, 2013, pp. 1–4.
- [12] M. Vergani, M. Carminati, G. Ferrari, M. Sampietro, L. Amato, A. Heiskanen, M. Dimaki, W. E. Svendsen, and J. Emneus, “Compact potentiostat for cellular electrochemical imaging with 54 parallel channels,” in *2012 IEEE Biomedical Circuits and Systems Conference (BioCAS)*, 2012, pp. 136–139.
- [13] A. A. Rowe, A. J. Bonham, R. J. White, M. P. Zimmer, R. J. Yadgar, T. M. Hobza, J. W. Honea, I. Ben-Yaacov, and K. W. Plaxco, “CheapStat: An Open-Source, ‘Do-It-Yourself’ Potentiostat for Analytical and Educational Applications,” *PLoS One*, vol. 6, no. 9, p. e23783, Sep. 2011.
- [14] M. H. Kim, I. Nam, Y. Ryu, L. W. Wellman, L. D. Sanford, and H. Yoon, “Miniaturized neural sensing and optogenetic stimulation system for behavioral studies in the rat,” 2015, p. 94340B.
- [15] A. Doholi, P. Kane, and D. Van Ess, “Dynamic reconfiguration in a PSoC device,” in *2009 International Conference on Field-Programmable Technology*, 2009, pp. 361–363.
- [16] P. Xuewei and A. K. Rathore, “Small-Signal Analysis of Naturally Commutated Current-Fed Dual Active Bridge Converter and Control Implementation Using Cypress PSoC,” *IEEE Trans. Veh. Technol.*, vol. 64, no. 11, pp. 4996–5005, Nov. 2015.
- [17] M. F. Masters, T. Heral, and K. Tummla, “Low-cost coincidence counting apparatus for quantum optics investigations,” 2015, p. 97930V.
- [18] G. Prasanna, J. Jayapandian, O. K. Sheela, and G. Amarendra, “A novel pulse processing scheme using embedded pulsed reset charge sensitive preamplifier,” 2016, p. 60023.
- [19] A. Bozatzidis, A. G. Anastopoulos, and T. Laopoulos, “An Automated Data Acquisition Setup for Electro-Chemical Measurements,” in *2007 4th IEEE Workshop on Intelligent Data Acquisition and Advanced Computing Systems: Technology and Applications*, 2007, pp. 51–54.
- [20] N. Pour Aryan, V. Rieger, C. Brendler, and A. Rothermel, “An Economical and convenient experiment setup for electrode investigation,” in *2012 Annual International Conference of the IEEE Engineering in Medicine and Biology Society*, 2012, pp. 815–818.
- [21] T. J. Bress, “Producer–Consumer State Machines,” in *Effective Labview Programming*, NTS Press, 2013, pp. 368–386.

- [22] C. M. A. Brett and A. M. O. Brett, "Electrochemical Experiments," in *Electrochemistry: principles, methods, and applications*, Oxford University Press, 1993, pp. 129–150.
- [23] J. Colomer-Farrarons and P. L. Miribel-Català, "Biomedical Integrated Instrumentation," in *A CMOS Self-Powered Front-End Architecture for Subcutaneous Event-Detector Devices*, Dordrecht: Springer Netherlands, 2011, pp. 93–132.
- [24] L. Li, X. Liu, W. A. Qureshi, and A. J. Mason, "CMOS Amperometric Instrumentation and Packaging for Biosensor Array Applications," *IEEE Trans. Biomed. Circuits Syst.*, vol. 5, no. 5, pp. 439–448, Oct. 2011.
- [25] L. Li, W. A. Qureshi, X. Liu, and A. J. Mason, "Amperometric instrumentation system with on-chip electrode array for biosensor application," in *2010 IEEE Biomedical Circuits and Systems Conference (BioCAS)*, 2010, pp. 294–297.
- [26] B. Lim, S. Takahashi, M. Futagawa, F. Dasai, M. Ishida, and K. Sawada, "On-chip square wave voltammetric pulse generator for redox measurement employing array structure," in *2014 IEEE Biomedical Circuits and Systems Conference (BioCAS)*, 2014, pp. 113–116.
- [27] M. Ciobanu, J. P. Wilburn, M. L. Krim, and D. E. Cliffel, "Fundamentals," in *Handbook of Electrochemistry*, Elsevier, 2007, pp. 1–30.
- [28] P. Zanello, "Voltammetric Techniques," in *Inorganic Electrochemistry: Theory, Practice and Applications*, Royal Society of Chemistry, 2003, pp. 49–138.
- [29] Allen. J. Bard and Larry. R. Faulkner, "Potential Sweep Methods," in *Electrochemical Methods: Fundamentals and Applications*, John Wiley & Sons (New York), 2001, pp. 226–260.
- [30] L. Bortels, B. Van den Bossche, J. Deconinck, S. Vandeputte, A. Hubinb, "Analytical solution for the steady-state diffusion and migration involving multiple reacting ions Application to the identification of Butler-Volmer kinetic parameters for the ferri-/ferrocyanide redox couple", *Journal of Electroanalytical Chemistry*, 429, 1997, pp. 139-155.
- [31] A. P. Periasamy, Y.-J. Chang, and S.-M. Chen, "Amperometric glucose sensor based on glucose oxidase immobilized on gelatin-multiwalled carbon nanotube modified glassy carbon electrode," *Bioelectrochemistry*, vol. 80, no. 2, pp. 114–120, 2011.
- [32] I. M. Apetrei and C. Apetrei, "Voltammetric determination of melatonin using a graphene-based sensor in pharmaceutical products.," *Int. J. Nanomedicine*, vol. 11, pp. 1859–66, 2016.
- [33] C. Chen, C. Sun, and Y. Gao, "Amperometric sensor for hydrogen peroxide based on poly(aniline-co-p-aminophenol)," 2009.
- [34] J. Duan, J. Duan, Z. Zhang, and T. Tong, "Irreversible cellular senescence induced by prolonged exposure to H<sub>2</sub>O<sub>2</sub> involves DNA-damage-and-repair genes and telomere shortening," *Int. J. Biochem. Cell Biol.*, vol. 37, no. 7, pp. 1407–1420, Jul. 2005.
- [35] C. Chen, X. Hong, T. Xu, A. Chen, L. Lu, and Y. Gao, "Hydrogen peroxide biosensor based on the immobilization of horseradish peroxidase onto a poly(aniline-co-N-methylthionine) film," *Synth. Met.*, vol. 212, pp. 123–130, 2016.
- [36] N. Jaiswal, I. Tiwari, C. W. Foster, and C. E. Banks, "Highly sensitive amperometric sensing of nitrite utilizing bulk-modified MnO<sub>2</sub> decorated Graphene oxide nanocomposite screen-printed electrodes," *Electrochim. Acta*, vol. 227, pp. 255–266, 2017.
- [37] H. M. Jafari, K. Abdelhalim, L. Soleymani, E. H. Sargent, S. O. Kelley, and R. Genov, "Nanostructured CMOS Wireless Ultra-Wideband Label-Free PCR-Free DNA Analysis SoC," *IEEE J. Solid-State Circuits*, vol. 49, no. 5, pp. 1223–1241, May 2014.

- [38] C. I. Dorta-Quinones, X. Y. Wang, R. K. Dokania, A. Gailey, M. Lindau, and A. B. Apsel, "A Wireless FSCV Monitoring IC With Analog Background Subtraction and UWB Telemetry," *IEEE Trans. Biomed. Circuits Syst.*, vol. 10, no. 2, pp. 289–299, Apr. 2016.
- [39] B. Bozorgzadeh, D. P. Covey, C. D. Howard, P. A. Garris, and P. Mohseni, "A Neurochemical Pattern Generator SoC With Switched-Electrode Management for Single-Chip Electrical Stimulation and 9.3  $\mu$ W, 78 pA rms, 400 V/s FSCV Sensing," *IEEE J. Solid-State Circuits*, vol. 49, no. 4, pp. 881–895, Apr. 2014.
- [40] "EmStat PalmSens." [Online]. Available: <http://www.palmsens.com/en/instruments/emstat/>. [Accessed: 03-Sep-2018].
- [41] "WaveNow Potentiostat/Galvanostat System – Pine Research Instrumentation". [Online]. Available: <https://www.pineresearch.com/shop/potentiostats/wavenow-series/wavenow-bundles/> [Accessed: 9-Sep-2018].
- [42] G. F. Giordano, M. B. R. Vicentini, R. C. Murer, F. Augusto, M. F. Ferrão, G. A. Helfer, A. B. da Costa, A. L. Gobbi, L. W. Hantao, and R. S. Lima, "Point-of-use electroanalytical platform based on homemade potentiostat and smartphone for multivariate data processing," *Electrochim. Acta*, vol. 219, pp. 170–177, 2016.